Self-Contained Resonant Rectifier for Piezoelectric Sources Under Variable Mechanical Excitation

Natan Krihely, *Student Member, IEEE*, and Shmuel (Sam) Ben-Yaakov, *Fellow, IEEE*

***Abstract*—A rectification scheme is proposed for increasing the available output power of electrical generators that have a high output capacitance. The proposed rectifier could be useful in increasing the output power of piezoelectric generators (PZG) that convert mechanical vibrations into electrical power. The improvement is achieved by a resonant circuit that self commutates the voltage across the output terminals of the PZG and thereby eliminates the shunting of the output current by the output capacitor. A low-consumption circuit synchronously controls the operation of the resonant rectifier by detecting voltage transitions across the generator. The presented resonant rectifier was experimentally verified by connecting it to a PZG as well as to a PZG emulator. The results show that, under constant harmonic excitation, the proposed circuit can significantly increase the extracted power by up to 230% as compared to a conventional bridge rectifier. The feasibility of using the proposed topology as a self-powered system driven by variable excitation was investigated experimentally as well. In particular, the system was driven by two types of excitation source: amplitude modulated and frequency modulated. It was found that the proposed circuit increases the extracted power by 160% and 172% for AM and FM excitations, respectively.**

***Index Terms*—Harvesting, piezoelectric (PZ) devices, resonant power conversion, synchronous detection.**

I. Introduction

PIEZOELECTRIC (PZ) elements can be used to generate electrical energy from mechanical energy. Such electrical generators could be useful in low-power applications, where mechanical motion is available. It has been shown, for example [1], that placing a PZ into a shoe sole can generate sufficient electrical power for sport sensors and a local microprocessor. Other demonstrated applications include a manually driven generator for portable radio receivers [2] and smart wireless sensing nodes capable of operation at extremely low-power levels [3]. PZ generators (PZGs) are very promising because of their high efficiency as compared to other methods [4]. However, effective use of these active generators requires a careful optimization in order to maximize the available output power. For example, matching the load to the device properties is mandatory in order to reach the maximum output power point [5]. Extensive research has been made in this area and several optimization circuits have been proposed [6].

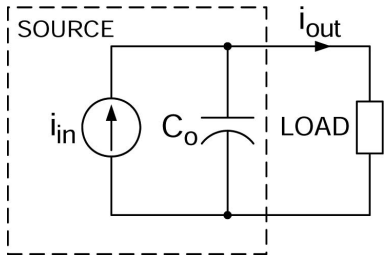

Fig. 1. Electrical equivalent circuit of capacitive current source driving a load.

PZ elements (PZG) belong to the general family of generators [7] that are characterized by an internal capacitive impedance. The vibrating PZ can be modeled as a sinusoidal current source $i_{\rm in}$ in parallel with its electrode capacitance C_o (see Fig. 1). The relatively low impedance of the internal capacitor shunts some of the output current and thereby lowers the available output power. Considerable effort has been made to reduce or even eliminate this drawback. The classical and intuitive solution is to shunt the capacitor with an external inductor, whose value is tuned to the frequency of the excitation. Consequently, the impedance of the *LC* resonant network is high and all the available power is dissipated in the load [8]. This technique typically requires a large inductance value (over 1 H), and is therefore an impractical solution. Another proposed solution is to emulate inductance behavior by a negative impedance [9]. In [10], the authors suggest the use of virtual grounded and floating inductors to achieve the required inductance value. However, these types of implementations are generally poor representations of ideal inductors, they are large in size, difficult to tune, sensitive to component variations, and require the inclusion of extra active elements in the circuit and an external power source. Considering the fact that, for a given excitation frequency, the inductance values are inversely proportional to the equivalent PZ capacitance, the required inductance can be reduced by simply increasing the capacitance [11]. This result is achieved by placing an additional external capacitor in parallel with the PZG. Indeed, the inductance value is significantly reduced, but so is the damping ratio. The high quality factor Q of this arrangement generates high reactive currents and makes the generator very sensitive to excitation frequency. The reactive current causes considerable power loss, and a slight change in frequency of the source causes a large power loss due to the shunting effect of the *LC* network.

In most applications, the ac signal produced by the PZG needs to be rectified [12]–[14]. However, considering the low-power

Manuscript received September 1, 2009; revised February 21, 2010; accepted April 27, 2010. Date of current version February 11, 2011. Recommended for publication by Associate Editor J. A. Cobos.

The authors are with the Power Electronics Laboratory, Department of Electrical and Computer Engineering, Ben-Gurion University of the Negev, Beer-Sheva 84105, Israel (e-mail: krikali@ee.bgu.ac.il; sby@ee.bgu.ac.il).

Color versions of one or more of the figures in this paper are available online at http://ieeexplore.ieee.org.

Digital Object Identifier 10.1109/TPEL.2010.2050336

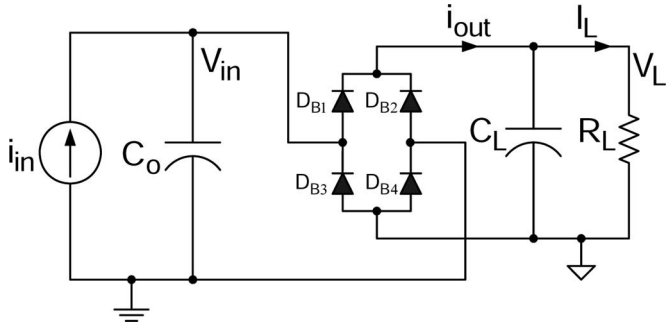

Fig. 2. General topology of a capacitive current source loaded by a conventional diode bridge rectifier circuit.

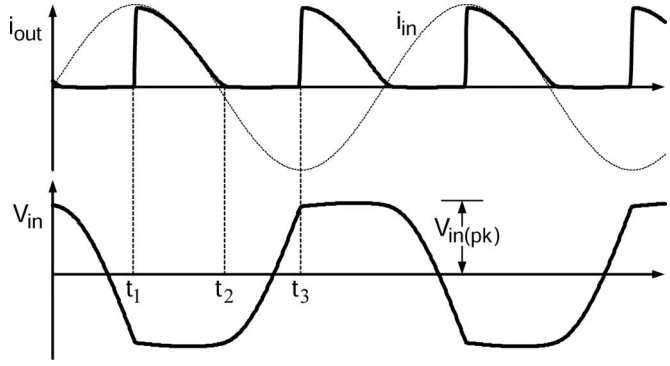

Fig. 3. Typical waveforms of diode bridge rectifier circuit.

level involved, the rectification scheme as well as the dc–dc converter used for impedance matching or voltage regulation [12]–[14] should be as efficient as possible in order to improve electrical power harvesting.

A basic rectification scheme (see Fig. 2) for an ac source such as the PZ generator includes a bridge rectifier or voltage doubler. Both suffer from output current loss due to the output capacitor C_o of the PZG. It has been shown that for such a rectification scheme, there is an optimum load resistance R_L for which the output power is maximized [14]–[16].

It was demonstrated in earlier studies that applying nonlinear power processing to the PZG can greatly enhance the electromechanical conversion and reduce the ill effect of the internal capacitor C_o. In particular, placing a switched inductor in different configurations along with the vibrating structure has been suggested in the literature [17]–[21]. The synchronized switch damping on inductor (SSDI) technique uses a PZG connected in series to an inductive circuit having an ON–OFF switch. The value (and size) of the inductor can be substantially lower than for the standard L shunt techniques mentioned earlier [8]–[11]. The required switching law of the SSDI has been implemented with a DSP [18], which makes the shunt circuit bulky and less efficient due to the extra power needed for its operation. Parallel synchronized switch harvesting on inductor (SSHI) technique proposed in [19] is similar to the SSDI method. This technique uses the inductive network (inductor plus switch) in parallel with the vibrating structure. The switch device is triggered on the maxima and minima of the PZ displacement, which requires the inclusion of an extra sensor, such as a proximity sensor, for its operation. It was stated in [19], without showing the actual circuitry, that a self-powered version of the electronic nonlinear processing circuit has been examined and that the power supply section consumed 5% of the processed power.

A similar technique called series SSHI has also been proposed in [20], while in [21], the series SSHI technique was introduced with only two diodes to further reduce power losses along the power flow path. However, the use of externally powered DSP makes the technique questionable for truly autonomous devices.

As stated previously, low-power harvesters usually require a two-stage conditioning circuit in order to make it compatible to different loads or storage devices such as supercapacitor [22]. This paper focuses on the optimization of the interaction between the first-stage rectification and a PZG. To this end, we fed a resistive load by the PZG through a modified diode bridge rectifier scheme. The power-optimization analysis is based on a simple lumped model of the PZG (see Fig. 1) driven by a steady and variable vibration around the resonance frequency of the unit under test. The contribution of this study is mainly for end applications that are intended for harvesting mechanical vibration energy, which exist for instance, on an office air conditioning unit or on a car engine. Other potential applications of the proposed circuit can be found in [6] and [23].

The objective of this study was twofold. First, to develop a sensor-free rectification scheme and low-consumption control circuit that improves the energy harvesting from a PZG by eliminating the shunting effect of the output capacitor. The second objective was to identify all lossy components in the proposed rectifier and derive the relevant relationships to estimate the loss budget. These loss calculations are essential not only for estimating the amount of power that can be obtained by a given interface circuit, but also for providing designers with basic information that can help optimize the system in terms of power loss.

II. Standard Diode Bridge Rectifier

Since the conventional diode bridge rectifier (see Fig. 2) is used as a reference for comparing the improvement of the new design, we first derive the expression for the maximum output power for this case taking into account the diodes' forward voltage drop V_D. The necessity for including V_D in the analysis comes from the nonnegligible losses introduced by the diode voltage drops in the case of low output voltage.

During the time interval t_1–t_2 (see Fig. 3), the capacitor C_o is clamped to the negative voltage $(-V_{\mathrm{in(pk)}})$ and provides a current path from the source to the load via D_{B2} and D_{B3} (see Fig. 2). The clamping voltage is equal to the sum of the dc output voltage V_L and two diode forward voltages V_D

$$V_{\mathrm{in(pk)}} = V_L + 2V_D. \tag{1}$$

During the time interval t_2–t_3 (see Fig. 3), the capacitor is charged by the current source, and the capacitor's voltage reverses its polarity from $-V_{\mathrm{in(pk)}}$ to $V_{\mathrm{in(pk)}}$. During this time period, no current is available to the load. The dc current that

reaches the load is the average of $i_{\rm out}$ (see Fig. 3)

$$I_L = \frac{2}{T_s}\int_0^{T_s/2} i_{\rm out}(t)dt = \frac{2}{T_s}\int_{t_1}^{t_2} |i_{\rm in}(t)|dt \qquad (2)$$

where T_s is the period of $i_{\rm in}$. One obtains

$$I_L = \left(\frac{2I_P}{\pi} - \frac{4\omega_s C_o V_D}{\pi}\right) \Big/ \left(1 + \frac{2\omega_s C_o R_L}{\pi}\right) \qquad (3)$$

where I_p and ω_s are the amplitude of the current and the resonant angular frequency of the current source, respectively. The power delivered to the load is thus

$$P_L(R_L) = \left[\left(\frac{2I_P}{\pi} - \frac{4\omega_s C_o V_D}{\pi}\right) \Big/ \left(1 + \frac{2\omega_s C_o R_L}{\pi}\right)\right]^2 R_L. \qquad (4)$$

Equations (3) and (4) are similar to the ones presented in [12] except that we included the contribution of the diodes to the losses.

The optimum load that maximizes the output power (taking into account the diode voltage drop) is the load that maximizes the power through the output load–diode combination

$$P_{\rm out} = P_L + P_D = I_L^2 R_L + 2V_D I_L. \qquad (5)$$

Differentiating (5) with respect to R_L and equating it to zero, we obtain

$$R_{L(\rm opt)} = \frac{\pi}{2} \cdot \frac{1}{\omega_s C_o\,(1 + 2V_D/V_L)}. \qquad (6)$$

Note that in the absence of capacitance C_o, the power is proportional to load resistance

$$P_L\ (R_L)|_{C_o=0} = \left(\frac{2I_P}{\pi}\right)^2 R_L \qquad (7)$$

and the power that can be extracted from the source theoretically approaches infinity (if R_L is made very high). In reality, the high output voltage generated when R_L is large dampens the PZ resonator and hence limits the output power [24].

III. Resonant Rectifier Circuit

The basic idea behind the proposed rectification scheme is to initiate self-commutation of the voltage across the output capacitor of the PZG. This is accomplished by connecting the output capacitor, with proper timing, to an inductor, which forms a resonant circuit with the capacitor and thereby causes the capacitor's voltage to flip polarity. The resonant rectification topology (see Fig. 4) includes an inductor ($L_{\rm res}$), two switches ($\rm SW_1$, $\rm SW_2$), two diodes (D_1, D_2), a differentiating circuitry that senses the slope of the capacitor's voltage (*dV/dt*), and a comparator (COMP.). A capacitor-loaded diode bridge rectifies the ac voltage across the PZG output capacitor ($V_{\rm in}$). The expected waveforms of the proposed rectifier over a complete cycle are presented in Fig. 5.

A. Principles of Operation

Assuming that at time t_1 (see Fig. 5), the capacitor C_o is precharged to $(-V_L–2V_D)$, the source current flows during $(t_1–t_2)$ to the load via D_{B2}, D_{B3}. At time instance t_2, the source

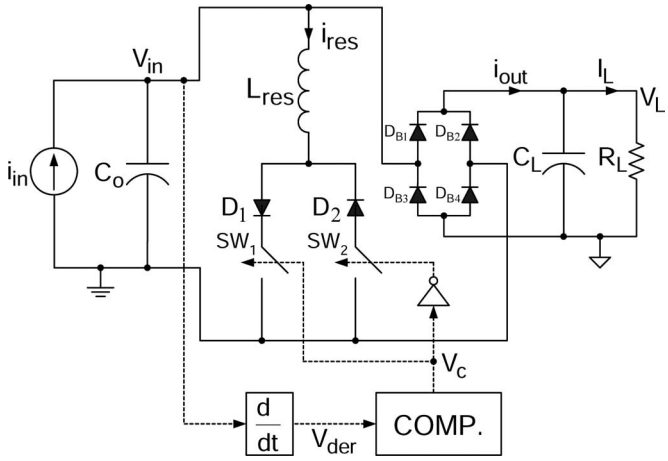

Fig. 4. Proposed resonant rectifier circuit.

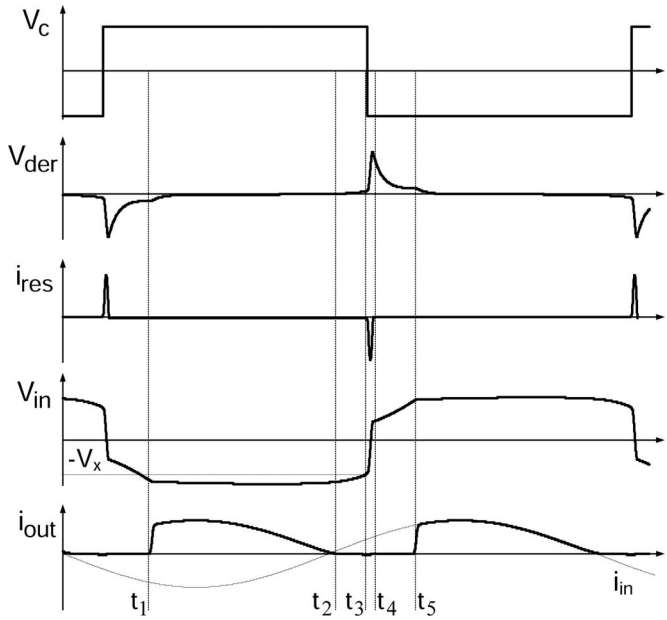

Fig. 5. Key waveforms of the resonant rectifier circuit.

current changes direction, starting to charge C_o during time t_2–t_3 until $V_{\rm der}$, i.e., the derivative of the capacitor's voltage $V_{\rm in}$ reaches the threshold level for the comparator causing its output (V_c) to switch to the low state at time t_3. This turns on switch $\rm SW_2$, which initiates a self-commutation interval t_3–t_4 via $\rm SW_2$–D_2–$L_{\rm res}$–C_o.

Assuming a high quality factor Q_r, the resonant time interval t_3–t_4 can be estimated as follows:

$$t_{\rm res} = t_4 - t_3 \approx \frac{\pi}{\omega_{\rm res}} = \pi\sqrt{L_{\rm res}C_o} \qquad (8)$$

and the peak current of $L_{\rm res}$ is

$$i_{\rm res(pk)} \approx \frac{V_{\rm in(pk)}}{Z_o} = V_{\rm in(pk)}\sqrt{\frac{C_o}{L_{\rm res}}} \qquad (9)$$

where

$$Z_o = \sqrt{\frac{L_{\rm res}}{C_o}}. \qquad (10)$$

While switch SW_2 is in the ON state, the instantaneous current $i_{\rm res}$ flowing through SW_2–D_2–$L_{\rm res}$–C_o during the charging resonance period t_3–t_4 satisfies

$$\begin{cases} L_{\rm res}\dfrac{di_{\rm res}}{dt} - V_D + i_{\rm res}R_r = V_{\rm in} \\ C_o\dfrac{dV_{\rm in}}{dt} = -i_{\rm res} \end{cases} \tag{11}$$

where R_r is the total resistance that includes $R_{\rm ds(on)}$ of the switches and the resistance of the inductor $R_{L\,(\rm res)}$.

The boundary conditions are: $i_{\rm res}(t_3) = 0$ and $V_{\rm in}(t_3) = -V_x$, where $-V_x$ stands for the voltage across C_o at time t_3 after being charged by the source $i_{\rm in}$ during t_2–t_3. Taking into account that $V_{\rm in} = -V_{\rm in(pk)}$ at t_2 and integrating the equation $i_{\rm in} = C_o(dV_{\rm in}/dt)$ from time t_2–t_3 gives

$$V_x = V_{\rm in(pk)} - \frac{I_P}{\omega_s C_o}(1 - \cos\omega_s t_D) \tag{12}$$

where the time interval t_2–t_3 is replaced for simplicity by the time interval 0–t_D such that $t_D = t_3 - t_2$.

Combining (11), (12), and the boundary conditions, yields

$$i_{\rm res}(t) = -\frac{V_x - V_D}{\omega_r L_{\rm res}}e^{-\alpha_r t}\cdot\sin\omega_r t. \tag{13}$$

α_r and ω_r are defined as follows:

$$\alpha_r = \frac{R_r}{2L_{\rm res}} \tag{14}$$

and

$$\omega_r = \sqrt{\omega_{\rm res}^2 - \alpha_r^2}. \tag{15}$$

$\omega_{\rm res}$ is the resonant angular frequency during the voltage inversion process

$$\omega_{\rm res} = \frac{1}{\sqrt{L_{\rm res}C_o}}. \tag{16}$$

The variation of $V_{\rm in}$ during the resonant period is obtained by substituting (13) into (11)

$$V_{\rm in}(t) = -\frac{V_x - V_D}{\omega_r L_{\rm res}}[(R_r - \alpha_r L_{\rm res})e^{-\alpha_r t}\sin\omega_r t + \omega_r L_{\rm res}e^{-\alpha_r t}\cos\omega_r t] - V_D. \tag{17}$$

At the end of the resonant period t_3–t_4, the reversed voltage becomes

$$V_{\rm in}(t_4) = V_x e^{-(\pi/2Q_r)} - V_D(1 + e^{-(\pi/2Q_r)}) \tag{18}$$

where $Q_r = \omega_r/2\alpha_r$ is the quality factor of the resonant branch.

During the time interval t_4–t_5, the inductor's current is already zero and the capacitor is charged by the input source current. There are two reasons for incomplete commutation. The first is the fact that commutation starts after the capacitor voltage has already dropped from $-V_{\rm in(pk)}$ to $-V_x$ during the interval t_2–t_3. Therefore, during the next interval (t_3–t_4), less energy is available and the capacitor voltage cannot be fully recovered to $V_L + 2V_D$. A second reason for incomplete commutation is the power loss during time duration (t_3–t_4) because of the voltage drop on D_2 and the resistance of $L_{\rm res}$, as well as the "ON" resistance of the switch (18). These power losses are replenished by the current coming from the source, and eventually, the input voltage $V_{\rm in}$ will be clamped to $V_L + 2V_D$ at time t_5 and a current path to the load is possible through diodes $D_{\rm B1}$ and $D_{\rm B4}$ of the bridge.

Thus, the operation of the resonant rectifier is based on the fact that the inductor and the PZG output capacitor form a resonant network that is activated by closing switches (SW_1) or (SW_2). The switches are closed at the end of each half cycle and thus the voltage across the capacitor will automatically, by virtue of the resonant current, change polarity. Consequently, except for the need to overcome losses, the PZG current is not required for commutating the capacitor voltage, and a larger portion of the current will pass to the output.

B. Loss Calculations

Losses due to R_r can be calculated as an integral over time of the instantaneous power

$$P_{R_r\,(\rm loss)} = \frac{2}{T_s}\int_{t_3}^{t_4} i_{\rm res}^2(t)R_r\,dt. \tag{19}$$

Hence, the estimated losses are

$$P_{R_r\,(\rm loss)} = f_s C_o(V_x - V_D)^2(1 - e^{-2\pi\frac{\alpha_r}{\omega_r}}). \tag{20}$$

The losses due to D_1 and D_2 are

$$P_{D\,(\rm loss)} = \frac{2}{T_s}\int_{t_3}^{t_4} i_{\rm res}(t)V_D\,dt. \tag{21}$$

Therefore,

$$P_{D\,(\rm loss)} = 2V_D f_s C_o(V_x - V_D)(1 + e^{-\pi\frac{\alpha_r}{\omega_r}}). \tag{22}$$

Losses in the comparator can be estimated by

$$P_{\rm Comp.(loss)} \approx 2V_{\rm in(pk)}I_Q \tag{23}$$

where I_Q is the bias current of the comparator.

Losses due to the parasitic gate capacitance of the switches are

$$P_{\rm Gate(loss)} \approx Q_{{\rm gs}(p)}V_{\rm in(pk)}f_s + Q_{{\rm gs}(n)}V_{\rm in(pk)}f_s \tag{24}$$

where $Q_{{\rm gs}(p)}$ and $Q_{{\rm gs}(n)}$ are the charges required to drive the gates of the switches to the final gate voltage level ($V_{\rm in(pk)}$ in our case).

The losses of the diode bridge are

$$P_{\rm Bridge(loss)} \approx 2V_D I_L. \tag{25}$$

The aforementioned expressions are used in the following section to estimate the losses of the proposed circuit and to compare them to experimental results.

IV. Experimental Results

The circuit diagram of the experimental set up is shown in Fig. 6. All the diodes used in the circuit are Schottky diodes (1N5817). The resonant circuit consisted of paralleled MOSFET switches (three VP0104 and three VN0104) for implementing M_p and M_n, respectively. The parallel structure is essential in order to reduce the relatively high drain-source resistance of

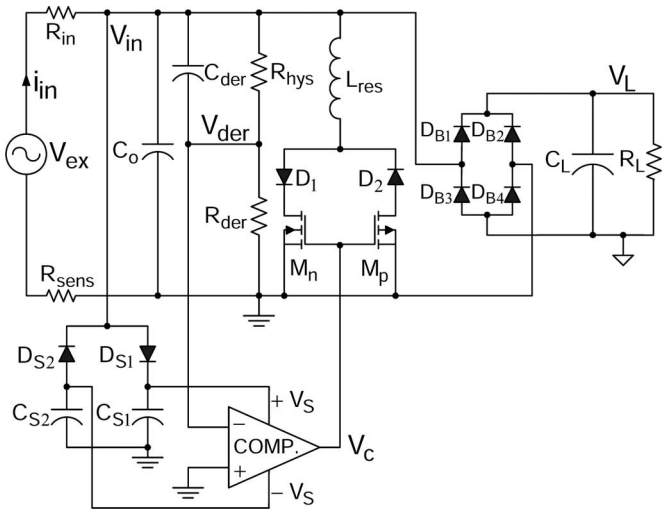

Fig. 6. Circuit diagram of experimental setup with dummy current source.

the MOSFETs. The $R_{\mathrm{ds(on)}}$ of the devices are of 3 and 11 Ω at a gate voltage of 5 V for the single *n* channel and *p* channel transistors, respectively. The parameters $Q_{\mathrm{gs}(p)}$ and $Q_{\mathrm{gs}(n)}$ are (from the data sheets of the devices): 3 × 0.3 nC and 3 × 0.4 nC, respectively. The 1-mH inductance of the resonant inductor L_{res} was built around an EFD 15 core (Philips), on which 35 turns of AWG #24 were wound. The series resistance of the inductor was measured by an *LCR* meter to be 0.24 Ω at a frequency of 1 kHz. The comparator was an ultralow power IC (MAX921, Maxim, USA) drawing 4-μA supply current I_Q. The bipolar power supply for the comparator was realized by two extra diodes (D_{S1}, D_{S2}) and bus capacitors (C_{S1}, C_{S2}).

The derivative of V_{in} (V_{der}) was obtained by a differentiator circuit $C_{\mathrm{der}} - R_{\mathrm{der}}$. In order to prevent either erroneous or undesired trigger events, hysteresis was introduced by adding resistor R_{hys}.

Three sets of experiments were performed as follows: (a) PZG emulator; (b) PZG under steady excitation; and (c) PZG under variable excitation.

A. PZG Emulator

The objective of this first set of experiments was to assess the performance of the proposed rectifier and to verify the loss calculation. In this setup, we used a dummy current source for modeling the generator stage. A high-voltage floating source V_{ex} of 200 $V_{(\mathrm{pk})}$ in series with 100-kΩ resistor R_{in} produced a sinusoidal current source i_{in} of 2 $\mathrm{mA}_{(\mathrm{pk})}$. This current was monitored by a 1-kΩ sense resistor R_{sens}. A capacitor C_o of 330 nF was placed in parallel to the input of the rectifier to emulate the capacitive behavior of the ac source.

The first measurement set included three rectification schemes: the standard diode bridge rectifier (see Fig. 2); the resonant rectifier (see Fig. 6); and the resonant rectifier, in which the comparator was fed by an auxiliary power supply (±4 V). The purpose of the third scheme was to neutralize the power consumption of the comparator and to ensure sufficient gate drive voltage to the MOSFETs. In each case, the load was adjusted to maximize the output power.

TABLE I
EXPERIMENTAL RESULTS WITH PZG EMULATOR

CIRCUIT TOPOLOGY	OUTPUT VOLTAGE (DC)	OPTIMAL LOAD	OUTPUT POWER	GAIN (%) COMPARED WITH STANDARD RECTIFIER
STANDARD RECTIFIER	1.6 V	2.1 kΩ	1.26 mW	-
RESONANT RECTIFIER	2.2 V	2.75 kΩ	1.79 mW	142%
RESONANT RECTIFIER WITH EXTERNAL SUPPLIES V_S=±4V	3.34 V	3.51 kΩ	3.16 mW	251%

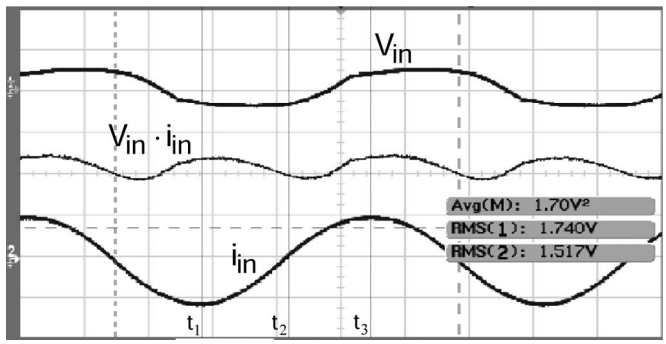

Fig. 7. Experimental waveforms of the standard rectifier. Measured input power: 1.7 mW. Vertical scales: $V_{\mathrm{in}} = 5$ V/div; and $i_{\mathrm{in}} = 2$ mA/div.

The results are summarized in Table I for the standard rectifier, self-powered resonant rectifier, and resonant rectifier with ±4 V external supplies. As expected, the latter yielded the highest power level of 3.16 mW, while the output of the standard rectifier was only 1.26 mW.

The resonant rectifier showed a significant improvement (251%) compared with conventional rectification output power. Figs. 7 and 8 show the experimental waveforms of the standard and resonant rectifiers with external supplies, respectively. Both figures are marked by the time events corresponding to those discussed in Sections II and III.

Neglecting comparator losses, total losses of the proposed circuit were estimated to be 1.143 mW for the experimental parameters: $t_D = 0.315$ ms; $V_{\mathrm{in(pk)}} = 3.5$ V; $L_{\mathrm{res}} = 1$ mH; $C_o = 330$ nF; $R_r = 1\ \Omega$; $V_D = 0.5$ V; $f_s = 185$ Hz; $C_L = 1\ \mu$F; and $I_L = 0.8$ mA. Based on the measured average input power of 3.96 mW [(see Fig. 8(a)] and the extracted output power of 3.16 mW (see Table I), the measured total loss of the resonant rectifier with external supplies is estimated to be 0.8 mW, which is lower than the estimated one.

B. PZG Under Steady Excitation

A second set of experiments was carried out by using a PZG (see Fig. 9) for the same three rectification circuits, while the testing procedure remained the same. The generator was built by connecting longitudinally two PZ bimorph van elements (RBL1–006 model, Piezo Systems, Inc., USA) with their centered shims glued together. One was used as an actuator and the other as a generator (see Fig. 10). The poling direction of

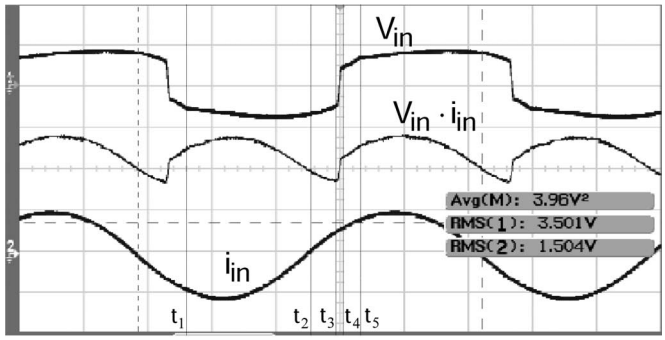

(a)

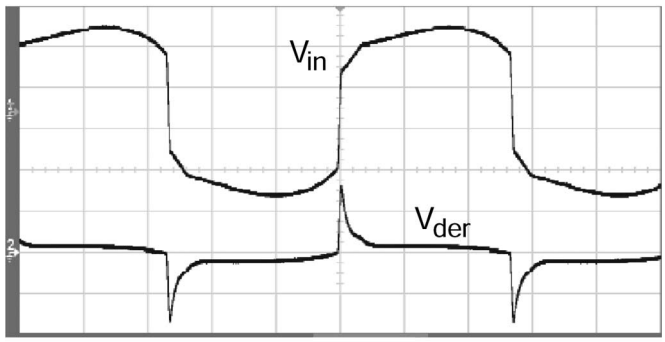

(b)

Fig. 8. Experimental waveforms of the proposed resonant rectifier. Measured input power: 3.96 mW. Vertical scales: (a) $V_{\rm in} = 5$ V/div; $i_{\rm in} = 2$ mA/div; and (b) 2 V/div.

Fig. 9. Experimental PZG (44.5 mm × 38.1 mm). Piezo Systems, Inc., USA.

the two PZ bimorph inserts is across the thickness dimension. Therefore, it is the lateral coupling k_{31}, which mainly drives the PZ response [25]. The actuator was excited by a sinusoidal voltage source of 40 $V_{\rm pk-pk}$. This arrangement provided the required mechanical excitation for the second van that was used as the generator. The output capacitance C_o of the PZG was estimated to be 60 nF using the technique of [26]. Two adjustments were needed here for maximizing the output power, one for locating the resonance frequency of the PZ device (approximately

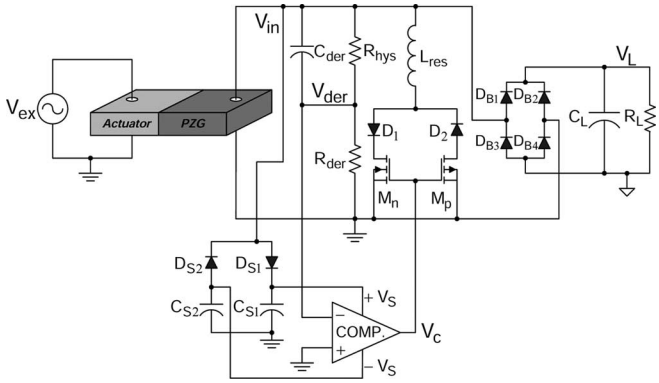

Fig. 10. Circuit diagram of experimental setup with PZG.

TABLE II
EXPERIMENTAL RESULTS WITH THE PZ G

CIRCUIT TOPOLOGY	OUTPUT VOLTAGE (DC)	OPTIMAL LOAD	OUTPUT POWER	GAIN (%) COMPARED WITH STANDARD RECTIFIER
STANDARD RECTIFIER	1.779 V	5.89 kΩ	0.537 mW	-
RESONANT RECTIFIER	1.818 V	5.19 kΩ	0.636 mW	**118%**
RESONANT RECTIFIER WITH EXTERNAL SUPPLIES V_S=±4V	3.75 V	11.43 kΩ	1.23 mW	**230%**

185 Hz), and the second adjustment for selecting the optimum load of the rectification circuit under test (for a given frequency). The measured extracted power for the three rectification circuits are summarized in Table II. Maximum extracted output power produced by the resonant rectifier with external supplies was 230% of the power produced by the conventional rectifier. The effective output power of the resonant rectifier with ±4 V external supplies case is actually lower than stated in Tables I and II. For an exact quantification, it is necessary to subtract the power consumption drawn from the external supplies and the damping loss factor associated with this power consumption (for the PZG case). The average current drawn from the power supplies was measured to be 4.4 μA, and the corresponding power consumption is 35.2 μW. The measured power consumption is in good agreement with the predicted value (33.55 μW) using the sum of (23) and (24).

C. PZG Under Variable Excitation

This section describes two experiments that were carried out using a PZG that was driven by another bimorph element of the same type, as introduced in the previous section. The yield of this PZG prototype was first experimentally calibrated by running the circuit as a self-powered resonant rectifier under constant excitation. A maximal extracted power of 0.378 mW was recorded, which implies a gain of 134% compared to a diode bridge rectifier. The experimental conditions were: sinusoidal excitation of 25 $V_{\rm pk-pk}$ at a frequency of 205 Hz. The gain of 134% is higher than the previous result (118%) specified in Table II. This can be probably explained by a better mechanical coupling between the generator and the actuator in this set

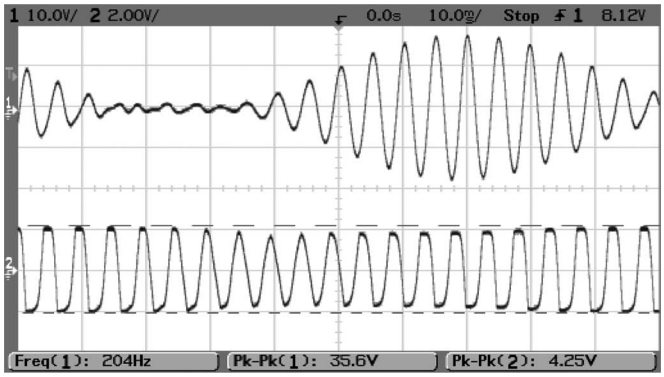

Fig. 11. Experimental waveforms of the PZG under AM excitation connected to the standard rectifier. $V_{\rm ex}$ (upper trace) and $V_{\rm in}$ (lower trace) (see Fig. 10).

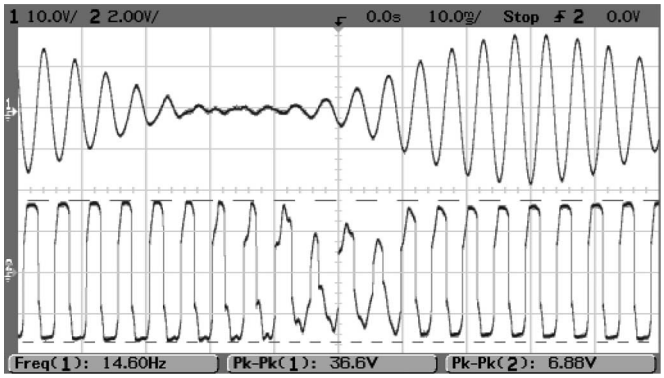

Fig. 12. Experimental waveforms of the PZG under AM excitation connected to the resonant rectifier. $V_{\rm ex}$ (upper trace) and $V_{\rm in}$ (lower trace) (see Fig. 10).

of experiments. The testing procedure in this section remained mainly the same, except that the actuating PZG was driven by a variable excitation source $V_{\rm ex}$ (see Fig. 10). The objective of this experiment was to investigate the ability of the resonant rectifier to operate in an environment with nonconstant mechanical vibrations as a self-powered unit. In these experiments, the third rectification scheme of the resonant rectifier with external supplies was omitted. To provide the required variable mechanical excitation, AM and FM were applied to the driving PZG. A nonconstant mechanical strain and off resonance conditions were created by AM and FM excitations, respectively. For each excitation signal and rectification scheme, the maximum power delivered to the load R_L was recorded.

The first measurement set was carried out by subjecting the actuator to an AM signal of 35 $V_{\rm pk-pk}$. The voltage excitation was set to this value to ensure that the rectified supply voltages ($\pm V_S$) of the comparator are below their maximum ratings ($\pm$5.5 V) for all possible loads. The carrier was tuned to the resonant frequency of the PZ structure $f_c \approx 205$ Hz, and the modulating signal was selected such that $f_c \gg f_m$ to $f_m = 12$ Hz. Figs. 11 and 12 show the experimental waveforms of the standard and the resonant rectifiers, respectively. Fig. 12 indicates that the resonant rectifier reverses the input voltage in the same manner, as under steady excitation (see Fig. 8). Specifically, this implies that the resonant rectifier is still able to effectively extract energy, even when the external excitation is very low.

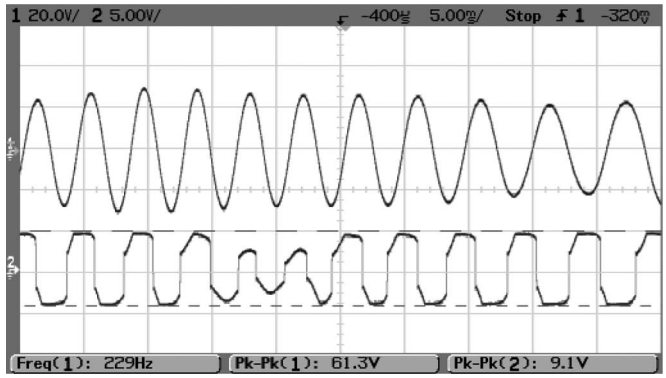

Fig. 13. Experimental waveforms of the PZG under FM excitation connected to the resonant rectifier. $V_{\rm ex}$ (upper trace) and $V_{\rm in}$ (lower trace) (see Fig. 10).

TABLE III
EXPERIMENTAL RESULTS OF THE PZG EXCITED BY AM AND FM WAVEFORMS

EXCAITATION MODE	TEST CONDITIONS	STANDARD RECTIFIER OUTPUT POWER	RESONANT RECTIFIER OUTPUT POWER	GAIN (%) COMPARED WITH STANDARD RECTIFIER
AM	f_c=205 Hz f_m=12 Hz V_{ex}=35 V_{pk-pk}	0.145 mW	0.233 mW	**160%**
FM	f_c=205 Hz Δf_m=40 Hz V_{ex}=60 V_{pk-pk}	0.198 mW	0.340 mW	**172%**

In the second measurement set, the system was driven by an FM signal with a fixed amplitude harmonic signal 60 $V_{\rm p-p}$ over a range of frequencies $\Delta f_m \approx 40$ Hz in the vicinity of the fundamental resonant frequency $f_c \approx 205$ Hz. The excitation level was raised since the PZG is essentially a resonant element that has low damping (high quality factor). Hence, it is expected that any slight deviation from resonance will result in sharp attenuation of the vibrations. Fig. 13 shows the experimental waveforms for FM excitation. Clearly, the proposed circuit is also functioning very well under this type of excitation. In this case, the amplitude changes at the input ($V_{\rm ex}$) and the output ($V_{\rm in}$) of the PZG are due to the high Q of the devices, which makes the vibrations strongly dependent on the deviation of the frequency from the resonant condition (see Fig. 13).

The measured maximum power for the two modes of excitation and the power gain compared to the standard rectifier are summarized in Table III. It was found that the proposed circuit can gain an extracted power of 160% and 172% for AM and FM excitations, respectively.

V. DISCUSSION AND CONCLUSION

A new resonant rectifier circuit is introduced. The operation of the circuit is based on highly efficient resonant energy transfer between a capacitive source such as a PZG and an inductor. This mechanism, controlled by self-timed circuitry, facilitates the commutation of the voltage across input capacitor C_o. This was shown to lead to a significant output power improvement of 251% compared to a conventional rectifier with a dummy source and 230% for a PZG.

The first experiment reveals total losses of 0.8 mW for the rectifier circuit with external supplies, while the theoretically estimated losses were 1.143 mW. The slight discrepancy

between the predicted and measured losses is probably due to the fact that in the calculation, it was assumed that the voltage drop across the diode is 0.5 V, while the actual drop, under the experimental conditions, is probably lower. Indeed, a considerable portion of the rectifier circuit losses is due to the forward voltage drop of the bridge diodes (D_B). The bridge diode losses are estimated to be [by (25)] 0.8 mW. The losses can be reduced by using a synchronous rectification scheme, in which the diodes (D_B) are replaced by a switch with low "ON" resistance to thereby reduce the forward voltage drop to a negligible value [27], [28].

The circuit was also tested in self-powered mode. It showed 142% output power improvement compared to the standard rectifier with dummy source, and 118% output power improvement with PZG. The main reason for this modest improvement is the low-power level that was available from the experimental PZG. One major reason for the power limitation in the experimental setup of this study is loading effects. In a typical harvesting application, the vibration source will have a much larger mass than the PZG, and the magnitude of the mechanical vibration will not be affected much when the generator is loaded, i.e., in these cases, the vibration source can be considered as an infinite source of power [29]. In the present study, the vibrating source was also a PZ van of the same dimensions as the generator. Even though the excitation element was driven by a constant voltage, the actual vibration was damped to a significant degree when the generator was electrically loaded. Consequently, the vibration amplitude decreased as the harvested electrical power increased. The relatively low-power level resulted in a low output and auxiliary supply voltages, which, in turn, was not sufficient to drive M_n and M_p into the range of low "ON" resistance $R_{\mathrm{ds(on)}}$. Specifically, according to Table II, the measured output voltage of the self-powered rectifier is approximately two times lower compared to the rectifier with external supplies (1.818 V versus 3.75 V) for the same V_{ex}. This low-voltage rail implies an increase in $R_{\mathrm{ds(on)}}$ level compared to the rectifier with external supplies. The dependency of the drain-source resistance on the gate-source voltage is given in the data sheets of the devices. Consequently, the decrease of the available power due to the damping effect caused an increase of power dissipation, which further reduced the available output power. It is thus expected that the output power will be considerable higher in applications, where the mechanical vibration source can be considered to be of "infinite power".

The total losses of the resonant rectifier are a function of the parasitic resistances and the voltage drop across the diode. The smaller the resistance and the voltage drops, the lower will be the losses. Optimization of the resonant inductor is less obvious. One might think that a reduction in inductance of value L_{res} will minimize the commutation period t_{res} (8), and hence will increase output power. In reality, a decrease in the value of L_{res} will increase the resonant current (9), which might lead to a larger power dissipation by D_1, D_2, M_n, M_p, and the resistance of the inductor, as shown in Fig. 14. This figure depicts the dependence of the sum $P_{R_r\,(\mathrm{loss})}+P_{D\,(\mathrm{loss})}$ [(20) and (22)] on the value of L_{res} while the other parameters are maintained constants. Therefore, in the selection of the inductor, one should consider two factors: the output power loss during the commutation period (t_{res}); and the power loss due to the resonant current i_{res} [(9) and (13)]. In practice, one should strive to make L_{res} as small as possible while keeping the conduction losses a reasonable fraction of the expected total power.

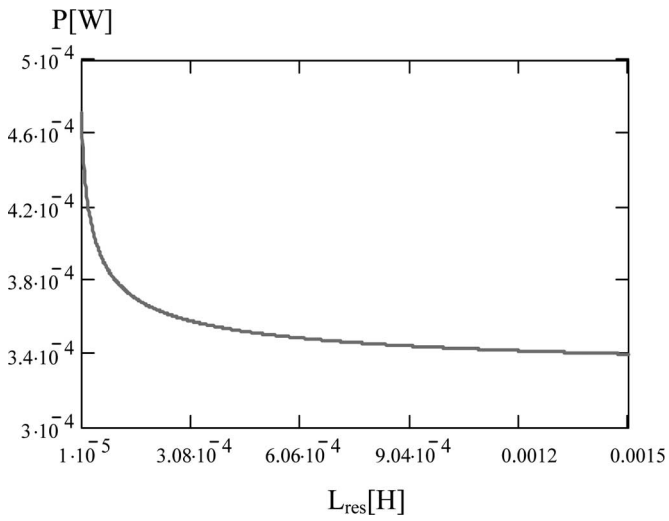

Fig. 14. Power losses calculated as sum $P_{R_r\,(\mathrm{loss})}+P_{D\,(\mathrm{loss})}$ as a function of L_{res} for: $f_s = 185$ Hz; $V_{\mathrm{in(pk)}} = 3.5$ V; $t_D = 0.315$ ms; $C_o = 330$ nF; $I_P = 2$ mA; $V_D = 0.5$ V, and $R_r = 1\ \Omega$.

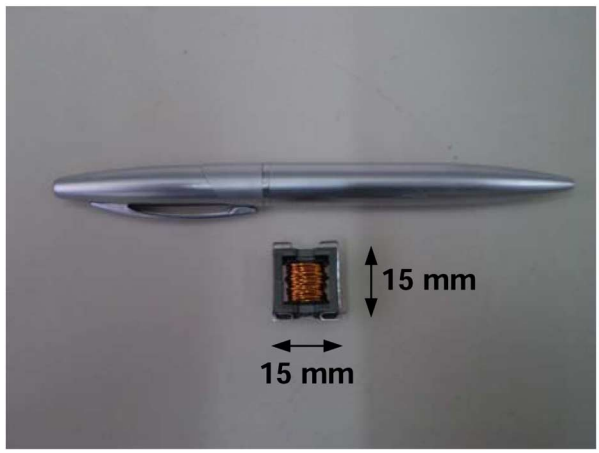

Fig. 15. Realization and the relative dimensions of a 1-mH resonant inductor: EFD 15 core (Philips), 35 turns of AWG #24. Dimensions of inductor: 15 mm × 15 mm.

The choice of the inductor used will in fact determine the size of the rectifier, since the rest of the electronics can be easily miniaturized by applying surface mount technology (SMT). However, as previously discussed, one needs to take into account the expected losses of the inductor. Although, very small commercially SMT inductors are available today [30], their accompanying DCR may easily exceed 1 Ω that could prevent the effectiveness of the system. In fact, to keep the losses low, one has to overspecify the inductor in terms of nominal current. The experimental resonant inductor used in this paper is depicted in Fig. 15.

It was shown experimentally that the resonant rectifier effectively converts mechanical power even under variable excitation. The experimental results reveal a power gain of 160% and 172% for AM and FM excitations compared to the standard diode bridge rectifier. This improvement reflects the control circuitry's ability to overcome temporary disturbances that the generator might be faced with. The results of these tests imply that the electrical energy generated by the PZG can be extracted even in a dynamically changing environment. The basis for this improvement stems from the fact that the voltage reversal of $V_{\rm in}$ is accomplished by the help of the inductor $L_{\rm res}$. Therefore, some electrical energy generated by the PZG can be extracted even in the "valley" points, which is considered as the region that the input voltage $V_{\rm in}$ has dropped (see Figs. 12 and 13). This cannot be accomplished by the standard rectifier because $i_{\rm in}$ alone is not sufficient to bring the voltage to a level that will initiate diode conduction.

As other sensor-free control topologies, the presented topology is not adaptive to the generator's parameters changes or different loads. The final application will integrate another stage for voltage regulation or impedance matching. Several approaches that apply dc–dc converter can be adopted [31]. By operating the converters in discontinuous conduction mode (DCM), they can be controlled to emulate at the input any desired equivalent resistance [13]. Matching this equivalent resistance to the optimal load of Table II will guarantee energy harvesting near maximum output power point. The type of the converter will be determined in this case by the nature of the source and the load. For example, due to low input voltage of a low-power rectifying antenna source [31], a boost converter is the logical choice. However, a buck–boost converter is capable to emulate an equivalent input resistance, which is independent of the voltage of the connected load [14].

Considering all the nonideal conditions and limitations previously discussed, the resonant rectifier exhibits an impressive improvement compared to the conventional rectifier. Additional improvement could be achieved by replacing the diode bridge by a synchronous rectification scheme in a self-powered system suitable for mobile applications. Future work will consider the integration of a second stage such as buck or buck–boost to the proposed circuit.

REFERENCES

[1] J. Kymissis, C. Kendall, J. Paradiso, and N. Gershenfeld, "Parasitic power harvesting in shoes," in *Proc. 2nd IEEE Int. Symp. Wearable Comput.*, 1998, pp. 132–139.

[2] J. M. Rabaey, M. J. Ammer, J. L. da Silva, D. Patel, and S. Roundy, "PicoRadio supports ad hoc ultra-low power wireless networking," *Comput.*, vol. 33, no. 7, pp. 42–48, July 2000.

[3] S. W. Arms, C. P. Townsend, D. L. Churchill, J. H. Galbreath, and S. W. Mundell, "Power management for energy harvesting wireless sensors," in *Proc. SPIE Int. Symp. Smart Struct. Smart Mater.*, San Diego, CA, 2005, vol. 5763, pp. 267–275.

[4] S. Roundy, P. K. Wright, and J. Rabaey, "A study oflow level vibrations as a power source for wireless sensor nodes," *Comput. Commun.*, vol. 26, pp. 1131–1144, 2003.

[5] E. S. Leland and P. K. Wright, "Resonance tuning of piezoelectric vibration energy scavenging generators using compressive axial preload," *Smart Mater. Struct.*, vol. 15, pp. 1413–1420, 2006.

[6] P. Shashank, "Advances in energy harvesting using low profile piezoelectric transducers," *J. Electroceramics*, vol. 19, no. 1, pp. 165–182, 2007.

[7] Catalog #7C, *Piezo Systems, Inc.*, 2008.

[8] W. Shu-Yau, "Piezoelectric shunts with a parallel R-L circuit for structural damping and vibration control," in *Proc. SPIE Smart Struct. Mater. Conf.*, Mar. 1996, vol. 2720, pp. 259–269.

[9] S. Behrens, A. J. Fleming, and S. O. R. Moheimani, "A broadband controller for shunt piezoelectric damping of structural vibration," *Smart Mater. Struct.*, vol. 12, pp. 18–28, 2003.

[10] F. dell'Isola, C. Maurini, and M. Porfiri, "Passive damping of beam vibrations through distributed electric networks and piezoelectric transducers: Prototype design and experimental validation," *Smart Mater. Struct.*, vol. 13, pp. 299–308, 2004.

[11] A. J. Fleming, S. Behrens, and S. O. R. Moheimani, "Reducing the inductance requirements of piezoelectric shunt damping systems," *Smart Mater. Struct.*, vol. 12, pp. 57–64, 2003.

[12] G. K. Ottman, H. F. Hofmann, A. C. Bhatt, and G. A. Lesieutre, "Adaptive piezoelectric energy harvesting circuit for wireless remote power supply," *IEEE Trans. Power Electron.*, vol. 17, no. 5, pp. 669–676, Sep. 2002.

[13] G. K. Ottman, H. F. Hofmann, and G. A. Lesieutre, "Optimized piezoelectric energy harvesting circuit using step-down converter in discontinuous conduction mode," *IEEE Trans. Power Electron.*, vol. 18, no. 2, pp. 696–703, Mar. 2003.

[14] A. Kasyap, J. Lim, D. Johnson, S. Horowitz, T. Nishida, K. Ngo, M. Sheplak, and L. Cattafesta, "Energy reclamation from a vibrating piezoceramic composite beam," presented at the 9th Int. Congr. Sound Vibr., Orlando, FL, Jul. 2002.

[15] F. Lu, H. P. Lee, and S. P. Lim, "Modeling and analysis of micro piezoelectric power generators for micro-electromechanical-systems applications," *Smart Mater. Struct.*, vol. 13, pp. 57–63, 2004.

[16] J. Han, A. V. Jouanne, T. Le, K. Mayaram, and T. S. Fiez, "Novel power conditioning circuits for piezoelectric micro power generators," in *Proc. IEEE Appl. Power Electron. Conf.*, 2004, pp. 1541–1546.

[17] S. Ben-Yaakov and N. Krihely, "New resonant rectifier for capacitive sources," in *Proc. 23rd IEEE Conv. Elect. Electron. Eng.*, Sep. 6–7, 2004, pp. 48–51.

[18] C. Richard, D. Guyomar, D. Audigier, and H. Bassaler, "Enhanced semi passive damping using continuous switching of a piezoelectric device on an inductor," in *Proc. SPIE Smart Struct. Mater. Conf., Passive Damping Isolation*, 2000, pp. 288–299.

[19] D. Guyomar, A. Badel, E. Lefeuvre, and C. Richard, "Toward energy harvesting using active materials and conversion improvement by nonlinear processing," *IEEE Trans. Ultrason., Ferroelect., Freq. Control*, vol. 52, no. 4, pp. 584–595, Apr. 2005.

[20] G. W. Taylor, J. R. Burns, S. A. Kammann, W. B. Powers, and T. R. Welsh, "The energy harvesting eel: A small subsurface ocean/river power generator," *IEEE J. Ocean. Eng.*, vol. 26, no. 4, pp. 539–547, Oct. 2001.

[21] K. Makihara, J. Onoda, and T. Miyakawa, "Low energy dissipation electric circuit for energy harvesting," *Smart Mater. Struct.*, vol. 14, pp. 1493–1498, 2006.

[22] Energy Harvesting, Texas Instruments White Paper, Texas Instruments, Nov. 2008. Available: www.ti.com/corp/docs/landing/cc430/graphics/slyy018_20081031.pdf

[23] R. Torah, P. Glynne-Jones, M. Tudor, T. O'Donnell, S. Roy, and S. Beeby, "Self-powered autonomous wireless sensor node using vibration energy harvesting," *Meas. Sci. Technol.*, vol. 19, pp. 1–8, 2008.

[24] G. A. Lesieutre, G. K. Ottman, and H. F. Hofmann, "Damping as a result of piezoelectric energy harvesting," *J. Sound Vibr.*, vol. 269, pp. 991–1001, Jan. 2004.

[25] S. Jiang, X. Li, S. Guo, Y. Hu, J. Yang, and Q. Jiang, "Performance of a piezoelectric bimorph for scavenging vibration energy," *Smart Mater. Struct.*, vol. 14, pp. 769–774, 2005.

[26] S. Ben-Yaakov and N. Krihely, "Modeling and driving piezoelectric resonant blade elements," in *Proc. IEEE Appl. Power Electron. Conf.*, 2004, pp. 1733–1739.

[27] T. T. Le, J. Han, A. von Jouanne, K. Mayaram, and T. S. Fiez, "Piezoelectric micro-power generation interface circuits," *IEEE J. Solid State Circ.*, vol. 41, no. 6, pp. 1411–1420, Jun. 2006.

[28] L. Chao, C. Y. Tsui, and W. H. Ki, "Vibration energy scavenging and management for ultra low power applications," *Proc. Int. Symp. Low Power Electron. Des.*, pp. 316–321, 2007.

[29] C. B. Williams and R. B. Yates, "Analysis of a micro-electric generator for microsystems," *in Proc. 8th Int. Conf. Solid-State Sens. Actuators, Eurosensors IX*, pp. 369–372, 1995.

[30] *SMT Power Inductors-MSS1260 Datasheet*, Coilcraft. Available: www.coilcraft.com/pdfs/mss1260.pdf
[31] T. Paing, J. Shin, R. Zane, and Z. Popovic, "Resistor emulation approach to low-power RF energy harvesting," *IEEE Trans. Power Electron.*, vol. 23, no. 3, pp. 1494–1501, May 2008.

Natan Krihely was born in Beer-Sheva, Israel, in 1975. He received the B.Sc. and M.Sc degrees in electrical engineering from Ben-Gurion University of the Negev, Beer-Sheva, in 2002 and 2006, respectively, where he is currently working toward the Ph.D. degree.

From 2006 to 2008, he was with Telkoor Power Supplies Ltd., where he was involved in the design of military power supplies. His current research interests include dc–dc converters, rectifiers, modeling and simulation, soft switching techniques, and energy harvesting.

Shmuel (Sam) Ben-Yaakov (M'87–SM'08–F'10) was born in Tel Aviv, Israel, in 1939. He received the B.Sc. degree in electrical engineering from the Technion, Haifa, Israel, in 1961, and the M.S. and Ph.D. degrees in engineering from the University of California, Los Angeles, CA, in 1967 and 1970, respectively.

He is currently an Emeritus Professor with the Department of Electrical and Computer Engineering, Ben-Gurion University of the Negev, Beer-Sheva, Israel, where he was the chairman from 1985 to 1989, and is presently the head of the Power Electronics Group (http://www.ee.bgu.ac.il/∼pel). His current research interests include power electronics, circuits and systems, electronic instrumentation, and engineering education. He is a Consultant to commercial companies on various subjects, including analog circuit design and power electronics.